Article

Discovery Medicine 2025; 37(200): 1991–2005
https://doi.org/10.24976/Discov.Med.202537200.171

Galectin-3 Mediates Ischemia-Reperfusion Injury Through Regulation of Oxidative Stress, Inflammation, and the TFAM/PPARβ Axis

Tingting Liu[1], Jing Wang[2,*]

[1]Department of Cardiovascular Medicine, Yantaishan Hospital, 264000 Yantai, Shandong, China
[2]Department of Cardiovascular Medicine, Central Hospital Affiliated to Shandong First Medical University, 250012 Jinan, Shandong, China
*Correspondence: jijiwang163@163.com (Jing Wang)

Submitted: 15 May 2025 Revised: 5 August 2025 Accepted: 22 August 2025 Published: 20 September 2025

Background: Ischemia-reperfusion (I/R) injury involves oxidative stress, inflammation, and mitochondrial dysfunction. Galectin-3 (Gal-3) plays a key regulatory role in these processes; however, its association with the Mitochondrial Transcription Factor A/Peroxisome Proliferator-Activated Receptor Beta (TFAM/PPARβ) signaling pathway remains unclear. Therefore, this study aims to investigate the role of Gal-3 in I/R injury, focusing on its impact on oxidative stress, inflammatory responses, and the TFAM/PPARβ signaling pathway. Furthermore, it explores the role of TFAM in Gal-3-mediated I/R injury.

Methods: A mouse I/R model was established, and recombinant Gal-3 protein or anti-Gal-3 antibody was injected to modulate Gal-3 expression. mRNA and protein levels of Gal-3 in mouse serum, as well as relevant oxidative stress and inflammation markers, were evaluated using quantitative Reverse Transcription Polymerase Chain Reaction (qRT-PCR), Western blotting, and histological analysis. The human myocardial AC16 cell line was used to establish an *in vitro* I/R model, and Sh-Gal-3 or Gal-3 overexpression plasmids were transfected to regulate Gal-3 expression, further assessing the effects of Gal-3 on oxidative stress and inflammatory response. Additionally, Sh-Gal-3 and Sh-TFAM were co-transfected into the I/R *in vitro* cell model to explore the role of TFAM in Gal-3-mediated effects.

Results: In the *in vivo* I/R model, compared to the Sham group, Gal-3 mRNA and protein levels were significantly increased in the serum of I/R mice ($p < 0.05$). Recombinant Gal-3 protein treatment aggravated myocardial injury, as evidenced by increased levels of Creatine Kinase-MB (CK-MB), Creatine Kinase (CK), Left Ventricular End-Diastolic Diameter (LVEDD), and Left Ventricular End-Systolic Diameter (LVESD), with a substantial increase in cardiac pathological damage. In contrast, anti-Gal-3 antibody treatment significantly alleviated these adverse effects. Masson staining revealed a significant increase in myocardial fibrosis in the I/R group, and Gal-3 further exacerbated fibrosis, which was counteracted by anti-Gal-3 treatment. Furthermore, the levels of pro-inflammatory cytokines and oxidative stress markers were significantly elevated in the I/R group, with administration of Gal-3 recombinant protein further enhancing these changes, while anti-Gal-3 treatment reduced them. In the *in vitro* model, Gal-3 overexpression significantly increased the levels of inflammatory factors and reactive oxygen species (ROS), whereas Gal-3 knockdown reduced these levels. After co-transfection of Sh-Gal-3 and Sh-TFAM, compared to the Sh-Gal-3 group, there was a significant increase in ROS fluorescence intensity, Malondialdehyde (MDA) levels, and 5,5′,6,6′-Tetrachloro-1,1′,3,3′-tetraethyl-imidacarbocyanine iodide (JC-1) disaggregation levels, while Superoxide Dismutase (SOD) levels were significantly reduced ($p < 0.05$). Additionally, the levels of Interleukin-6 (IL-6), Interferon-gamma (IFN-γ), and Tumor Necrosis Factor-alpha (TNF-α) in the Sh-Gal-3+Sh-TFAM group were significantly higher than those in the Sh-Gal-3 group.

Conclusions: This study demonstrates that Gal-3 plays a crucial role in I/R injury, promoting oxidative stress, inflammation, and myocardial damage, by modulating the TFAM/PPARβ signaling pathway. Furthermore, TFAM plays a critical regulatory role in Gal-3-mediated oxidative stress and inflammation. These findings provide new insights into treating I/R injury, and targeting Gal-3 and TFAM may offer a potential therapeutic strategy for I/R-induced injury.

Keywords: galectin-3; myocardial ischemia-reperfusion injury; TFAM/PPARβ; oxidative stress; inflammatory response

Introduction

Myocardial ischemia-reperfusion (I/R) injury is a common and highly lethal pathological process in cardiovascular diseases, frequently observed in clinical scenarios such as acute myocardial infarction (AMI), coronary artery bypass grafting (CABG), and other cardiac surgeries [1–3]. During I/R injury, myocardial cells first undergo disturbances in energy metabolism caused by ischemia. Upon reperfusion, the restoration of blood flow and oxygen supply induces a series of adverse responses, including oxidative stress and inflammation, which further increase myocardial damage [4,5]. These detrimental responses not only disrupt cell membranes, proteins, and DNA but also cause myocardial cell death, tissue necrosis, and a significant loss of cardiac function [6,7]. The cardiac remodeling, including fibrosis, ventricular dilation, and heart failure, frequently leads to poor clinical outcomes and prognosis [8,9]. Therefore, exploring the molecular mechanisms driving I/R injury and identifying new therapeutic targets are crucial for improving treatment outcomes and patient prognosis.

Oxidative stress and inflammation are recognized as two key pathological drivers of I/R injury [10]. During ischemia, metabolic disturbances in myocardial cells under anaerobic conditions lead to a rapid decline in ATP levels and the accumulation of harmful metabolites [11]. Upon reperfusion, the sudden influx of oxygen produces a significant amount of reactive oxygen species (ROS), which activate multiple signaling pathways, exacerbating damage to the cell membrane, mitochondria, and endoplasmic reticulum, and ultimately triggering cell death [12]. Studies have revealed that oxidative stress and inflammation reinforce each other, promoting the occurrence and progression of I/R injury [13,14]. Therefore, inhibiting the excessive activation of both responses is crucial for alleviating I/R-induced myocardial injury.

Galectin-3 (Gal-3) is a multifunctional β-galactose-binding glycoprotein highly expressed in various tissues, such as the heart, liver, and immune cells [15]. Recent evidence has shown that Gal-3 plays an important role in cardiovascular diseases, especially in myocardial ischemia, inflammation, fibrosis, and heart failure [16]. In cardiac injury, Gal-3 promotes further myocardial damage by increasing inflammation, exacerbating oxidative stress, and modulating myocardial fibrosis [17]. Notably, evidence indicates that Gal-3 can exacerbate myocardial injury during I/R by affecting immune cell activity and inflammatory responses [18]. Despite this evidence, the specific role of Gal-3 in I/R injury and the underlying molecular mechanisms, particularly regarding the interaction between oxidative stress and inflammation, remain unclear.

The central roles of oxidative stress and inflammation in I/R injury have been well recognized [19]. ROS is the key mediator of I/R injury, with excessive ROS causing damage to cell membranes, activating inflammatory pathways, and disrupting mitochondrial activity [20]. However, oxidative stress is not only driven by ROS production but also closely related to the imbalance in intracellular antioxidant systems. Gal-3, as a crucial regulatory molecule, can exacerbate oxidative stress by enhancing ROS generation while reducing the activity of antioxidant enzyme [21]. For example, Li *et al*. [22] reported that inhibition of Proprotein Convertase Subtilisin/Kexin Type 9 (PCSK9) alleviates I/R-induced cardiac remodeling and dysfunction through LIAS-mediated cuproptosis, highlighting the critical role of immune signaling in modulating oxidative stress and inflammatory responses. Additionally, Gal-3 promotes the release of pro-inflammatory cytokines and increases the infiltration of inflammatory cells, thereby enhancing myocardial damage [23].

The role of mitochondria in I/R-induced myocardial injury cannot be ignored. Mitochondria are not only the core of cellular energy metabolism but also involved in ROS production and the regulation of oxidative stress [24]. Mitochondrial transcription factor A (TFAM) and peroxisome proliferator-activated receptor β (PPARβ) are crucial regulators of mitochondrial function and energy metabolism [25]. TFAM maintains mitochondrial DNA stability and ensures efficient mitochondrial energy production, whereas PPARβ regulates fatty acid oxidation and antioxidant stress. Research has shown that TFAM may exert its protective effects on mitochondria via modulating the PPARβ signaling pathway [25]. Dysregulation of the TFAM/PPARβ signaling axis has been closely associated with oxidative stress and inflammatory responses in myocardial I/R injury, making it a potential therapeutic target. However, whether Gal-3 exacerbates myocardial injury by regulating the TFAM and PPARβ signaling pathways remains to be fully explored.

This study aims to investigate the complex regulatory interplay between Gal-3 and the TFAM/PPARβ signaling axis, which is yet to be fully elucidated, and examine how this interaction influences mitochondrial homeostasis during I/R injury. By exploring this mechanism, our study provides novel mechanistic insights that differentiate it from earlier studies and enhance our understanding of the molecular processes involved in myocardial I/R injury.

Materials and Methods

I/R Animal Model

Male C57BL/6 mice (n = 28), aged 6–8 weeks and weighing 26 $\pm$ 2 g, were purchased from Vital River (Beijing, China). Animals were housed under controlled conditions with a temperature of 20–25 °C, relative humidity of 50%–60%, and a 12-hour light-dark cycle. Mice were fasted for 12 hours before experiments, with free access to water. Anesthesia was induced through intraperitoneal injection of sodium pentobarbital (40 mg/kg) (57-33-0, Sigma-Aldrich, St. Louis, MO, USA).

The mice were randomly divided into 4 groups using a random number table method: a Sham group (n = 7), an I/R group (n = 7), an I/R+Gal-3 group (n = 7), and an I/R+anti-Gal-3 group (n = 7). A midline incision was made through the skin and muscle to access the thoracic cavity. The sternum was carefully cut to expose the heart. Through microsurgery, the coronary artery was visualized, and the left anterior descending artery (LAD) was selected for model establishment. The coronary artery was occluded using a catheter, interrupting blood flow, which led to localized pallor in the ischemic myocardial area and significant cardiac dysfunction. Occlusion was maintained for 30 minutes, after which the catheter was removed to restore blood flow and begin reperfusion for 4 hours. Two hours after reperfusion, mice were intraperitoneally injected with recombinant human Gal-3 protein, Gal-3 antibody, or normal saline, depending on the specific group. Group-specific treatments were provided as follows:

I/R group: Mice in this experimental group underwent standard myocardial ischemia-reperfusion procedures and received an intraperitoneal injection of an equal volume of normal saline.

Sham group: Mice in this group received similar surgical procedures without coronary artery occlusion; the heart was exposed, but no ischemic injury was induced. Moreover, they received an intraperitoneal injection of an equal volume of normal saline.

I/R+Gal-3 group: Mice were injected intraperitoneally with recombinant human Gal-3 protein (10 µg/3 days) (ab50236, Purity ≥98%, Abcam, Cambridge, UK) for 4 weeks.

I/R+anti-Gal-3 group: Mice were injected intraperitoneally with human anti-Gal-3 antibody (5 µg/3 days) (ab76245, Purity ≥98%, Abcam, Cambridge, UK) for 4 weeks.

After 4 weeks of treatment, the mice were euthanized with an intraperitoneal injection of 3% sodium pentobarbital (110 mg/kg).

Heart tissue and venous blood were collected from each group of mice. All subsequent assessments, including biochemical analysis, histological evaluation, and data interpretation, were performed by independent investigators who were blinded to the group assignments to ensure objectivity. During surgery, mice were maintained on a temperature-controlled heating pad to keep their body temperature around 37 °C. After reperfusion, mice were closely monitored and carefully managed. Postoperatively, they were housed individually in cages with soft bedding and provided with analgesics when necessary to alleviate discomfort. Postoperative analgesia was administered through subcutaneous injection of meloxicam at a dose of 3 mg/kg.

Throughout the study, one mouse in the I/R group died on postoperative day 3, while no deaths occurred in the Sham group. In the I/R+Gal-3 group, one mouse died on day 1 and another on day 3 after surgery. However, no deaths were observed in the I/R+anti-Gal-3 group. Mice that died due to surgical complications were excluded from the final analyses. The overall survival rate across all groups was over 90%.

This study was approved by the Animal Ethics Committee of Binzhou Medical University (Approval No.: 2025-280), with experimental designs adhering to the institutional guidelines.

Quantitative Real-Time Polymerase Chain Reaction (qRT-PCR)

Total RNA was extracted from cells or tissue samples using TRIzol reagent (R1100, Solarbio, Beijing, China), and RNA concentration and purity were determined. Complementary DNA (cDNA) was synthesized from 1 µg of total RNA using reverse transcriptase (K16325, Fermentas, Burlington, Ontario) with either random primers or oligo(dT) primers. The qPCR reaction was conducted using SYBR Green PCR Master Mix with specific primers in a thermal cycler (CFX96, Bio-Rad, Hercules, CA, USA). The reaction conditions included an initial denaturation at 95 °C for 2–3 minutes, followed by 40 cycles of 95 °C for 15 seconds (denaturation), 60 °C for 20 seconds (annealing), and 72 °C for 30 seconds (extension). A melt curve analysis was performed at the end of the reaction to confirm the specificity of the PCR product. Relative gene expression levels were determined using the $2^{-\Delta\Delta Ct}$ method, with the Ct values normalized to the housekeeping gene GAPDH. Primer sequences used in this study are listed in Table 1.

Table 1. Primer sequences used in qRT-PCR.

Primer name	Primer sequences
Mus-Gal-3-F	TAATCAGGTGAGCGGCACAG
Mus-Gal-3-R	TAGGTGAGCATCGTTGACCG
Mus-IFN-γ-F	CGGCACAGTCATTGAAAGCC
Mus-IFN-γ-R	TGCATCCTTTTTCGCCTTGC
Mus-TNF-α-F	ACCCTCACACTCACAAACCA
Mus-TNF-α-R	ACCCTGAGCCATAATCCCCT
Human-Gal-3-F	CCATTTGAAAGTGGGAAACCA
Human-Gal-3-R	CATCATTCACTGCAACCTTGAAG
Human-IFN-γ-F	TCGGTAACTGACTTGAATGTCCA
Human-IFN-γ-R	TCGCTTCCCTGTTTTAGCTGC
Human-TNF-α-F	GGGACCTCTCTCTAATCAGCCCT
Human-TNF-α-R	GGCTTGTCACTCGGGGTTCG
Mus-GAPDH-F	TGTCTCCTGCGACTTCAACA
Mus-GAPDH-R	GGTGGTCCAGGGTTTCTTACT
Human-GAPDH-F	TGCACCACCAACTGCTTA
Human-GAPDH-R	GGATGCAGGGATGATGTTC

qRT-PCR, quantitative Reverse Transcription Polymerase Chain Reaction; Gal-3, galectin-3; IFN-γ, Interferon-gamma; TNF-α, Tumor Necrosis Factor-alpha; GAPDH, Glyceraldehyde-3-Phosphate Dehydrogenase.

Western Blotting

Total proteins were extracted from cells or tissue samples using RIPA buffer (R0010, Solarbio, Beijing, China), and quantified using a BCA assay kit (PC0020, Solarbio, Beijing, China) to ensure a consistent protein concentration across samples. Extracted proteins were mixed with protein loading buffer and denatured by heating. Proteins were then resolved through SDS-PAGE (P1200, Solarbio, Beijing, China) using a 12% polyacrylamide gel, and subsequently transferred onto a PVDF membrane (YA1701, Solarbio, Beijing, China) through electroblotting. Protein transfer efficiency was verified using Ponceau S staining. The membrane was blocked with 5% BSA (SW3015, Solarbio, Beijing, China) to prevent nonspecific binding. Membranes then underwent 1-hour incubation at room temperature with specific primary antibodies (Gal-3 (1:1000, ab76245, Abcam, Cambridge, UK), PPARβ (1:1000, ab178866, Abcam, Cambridge, UK), TFAM (1:1000, 23996-1-AP, Proteintech, Wuhan, China), GAPDH (1:1000, ab9485, Abcam, Cambridge, UK)). After three TBST washes to remove any unbound primary antibody, membranes were incubated with an HRP-conjugated secondary antibody (1:1000, ab6721, Abcam, Cambridge, UK) for 1 hour. Finally, protein bands were developed using an ECL reagent (P0018S, Beyotime, Beijing, China), and signals were captured with a chemiluminescence imaging system (GelDoc EZ, Bio-Rad, Hercules, CA, USA). The expression levels of the target protein were quantified using GAPDH as an internal control, and protein band intensities were analyzed using Image J software (version 1.5f, NIH, Bethesda, MD, USA).

Enzyme-Linked Immunosorbent Assay

Heart tissues from the experimental mice were collected, rapidly frozen, and stored at –80 °C. Before analysis, the tissues were homogenized to extract total proteins or other required components. Cell culture supernatants were collected and centrifuged at 3000 rpm for 10 minutes to remove cell debris. Commercially available kits were employed to assess corresponding biochemical markers: CK-MB (JL12422, JONLNBIO, Shanghai, China), CK (JL18284, JONLNBIO, Shanghai, China), Interleukin-1 beta (IL-1β) (JL18442, JONLNBIO, Shanghai, China), IL-6 (JL20268, JONLNBIO, Shanghai, China), MDA (JL53632, JONLNBIO, Shanghai, China), Superoxide Dismutase (SOD) (JL12237, JONLNBIO, Shanghai, China), Glutathione (GSH) (JL-T0906, JONLNBIO, Shanghai, China), Human IL-6 (JL14113, JONLNBIO, Shanghai, China), Human IL-1β (JL13662, JONLNBIO, Shanghai, China). Working solutions and standard curves were prepared following the manufacturer's instructions. Finally, absorbance reading of each sample was determined using a microplate reader (ELx800, BioTek, Winooski, VT, USA) at the following wavelengths: CK-MB and CK at 340 nm, IL-1β and IL-6 at 450 nm, MDA at 532 nm, SOD at 550 nm, and GSH at 412 nm.

Echocardiography

The mouse was positioned supine on a warm surface, exposing the chest area. An appropriate amount of ultrasound coupling gel was applied to the skin of the chest to ensure optimal acoustic contact. Imaging was performed using a high-frequency small animal echocardiography system (Vevo series, FUJIFILM VisualSonics Inc., Toronto, Ontario), with a probe suitable for mice (typically a 25 MHz probe). Device settings were adjusted to capture clear 2D images for accurate measurement of various cardiac parameters. LVEDD, LVESD, Left Ventricular Ejection Fraction (LVEF), and Left Ventricular Fractional Shortening (LVFS) were measured. Echocardiographic assessment was performed 24 hours after I/R modeling to evaluate cardiac function.

Hematoxylin and Eosin Staining

Heart tissues were fixed in 4% paraformaldehyde for 24 hours and then embedded in paraffin. Using a microtome, the tissues were sectioned into 5-µm-thick slices. The slices were immersed in xylene to remove the paraffin and were gradually dehydrated through a series of graded ethanol solutions. Hematoxylin and Eosin Staining (HE) staining was performed using a commercial kit (G1120, Solarbio, Beijing, China). The tissue sections were then stained with a hematoxylin solution for additional 5 minutes, followed by eosin staining for 5 minutes. Following staining, the slices were dehydrated through a graded ethanol, cleaned with xylene, and mounted with a transparent medium under a coverslip. Finally, the sections were observed under a microscope (CX23, Olympus, Tokyo, Japan), and images were quantitatively analyzed using ImageJ software (version 1.5f, NIH, Bethesda, MD, USA).

Masson Staining

Fixed tissue samples were sectioned into 5 µm thick slices and mounted onto glass slides, then dried in an oven at 60 °C. Paraffin was removed by immersing the slices in xylene, followed by dehydration through a graded ethanol, and finally slices were washed with distilled water. Masson's trichrome staining was conducted using a commercially available kit (G1340, Solarbio, Beijing, China). Tissue sections were initially stained with hematoxylin for 5 minutes and washed with running water to remove excess dye. Sections were then immersed in Biebrich Scarlet solution for 3 minutes, rinsed with running water, and subsequently stained with Phosphotungstic Acid-Acid Orange solution for 5 minutes, followed by another rinse. After staining, the slices are dehydrated through a graded ethanol series, cleared with xylene, and mounted with a transparent medium under a coverslip. Then, the stained tissue sections were observed under a microscope (CX23, Olympus, Tokyo, Japan), where collagen fibers appear blue or green, cytoplasm appears red or pink, and muscle tissue

appears red. Quantitative analysis of the stained images was performed using ImageJ software (version 1.5f, NIH, Bethesda, MD, USA).

Cell Culture

The AC16 human cardiac cell line (iCell-h323) was obtained from Cellverse Co., Ltd. (Shanghai, China) and cultured in DMEM medium (iCell-0001, Cellverse Co., Ltd., Shanghai, China) containing 10% fetal bovine serum (FBS) and 1% penicillin-streptomycin. Cell culture was maintained at 37 °C in a 5% CO_2 environment. Cell culture was authenticated by STR profiling and examined for mycoplasma contamination.

Establishment of the I/R In Vitro Model

For the *in vitro* I/R model, AC16 human cardiomyocyte cells in the logarithmic growth phase were washed twice with PBS and incubated with serum- and glucose-free DMEM to simulate ischemic conditions. The cells were incubated under hypoxic conditions in a tri-gas incubator (1% oxygen, 5% carbon dioxide and 94% nitrogen) at 37 °C for 4 hours. Following the ischemic period, cells were returned to normoxic conditions (21% O_2, 5% CO_2, 74% N_2) and cultured in complete DMEM containing 10% FBS and 4.5 g/L glucose for 2 hours to simulate reperfusion.

Cell Transfection

The established I/R *in vitro* cell model was cultured to reach the maximum confluence. Gal-3 overexpression plasmids, ShRNA-NC (TTCTCCGAACGTGTCACGT), ShRNA(Gal-3)-1 (GCAGTACAATCATCGGGTTAA), ShRNA(Gal-3)-2 (CCCACGCTTCAATGAGAACAA), ShRNA(Gal-3)-3 (GCAAACAGAATTGCTTTAGAT), ShRNA(TFAM)-1 (GCAAGCTGAAGAGATGAGAT), ShRNA(TFAM)-2 (GCACCTGATGTGGACCTATT), ShRNA(TFAM)-3 (GCTGCTTTCTACCAAGGAAT) were cloned into the pLKO.1-puro lentiviral vector. Gal-3 overexpression plasmid (ctggcgcatgggggaaccagcctgctgggg caggggctacccaggggcttcctatcctggggcctaccccgggcaggcaccc ccaggggcttatcctggacaggcacctccaggcgcctaccctggagcacctgg agcttatcccggagcacctgcacctggagtctacccagggccacccagcggcc ctggggcctacccatcttctggacagccaagtgccaccggagcctaccctgcca ctggcccctatggcgcccctgctgggccactgattgtgccttataacctgcctttg cctggcgcatgggggaaccagcctgctggggcaggggctacccaggggctt cctatcctggggcctaccccgggcaggcacccccaggggcttatcctggacag gcacctccaggcgcctaccctggagcacctggagcttatcccggag), overexpression control (NC), ShRNA(NC), ShRNA(TFAM), or ShRNA(Gal-3) were mixed with Lipofectamine 6000 transfection reagent (C0526, Beyotime, Shanghai, China), following the manufacturer's instructions. The transfection complex was added to the I/R cell model cultures. After 10 hours, the culture medium was refreshed with complete medium, and transfection efficiency was assessed 48 hours post-transfection.

Flow Cytometry

Mitochondrial integrity was evaluated using a 5,5′,6,6′-Tetrachloro-1,1′,3,3′-tetraethylimidacarbocyanine iodide (JC-1) mitochondrial membrane potential detection kit (C2003S, Beyotime, Shanghai, China). Logarithmically growing cells (~1 × 10^6 per group) were collected, washed with pre-warmed PBS, and resuspended in serum-free medium or the JC-1 assay buffer provided in the kit. JC-1 working solution was prepared according to the manufacturer's instructions and added to the cell suspension. The cells were incubated at 37 °C in the dark for 30 minutes, with gentle mixing every 10 minutes. After incubation, cells were washed once with PBS, centrifuged for 5 minutes, and the supernatant was discarded. The cell pellet was then resuspended in detection buffer. Mitochondrial membrane potential was assessed with flow cytometry (FACSCanto II, BD Biosciences, Franklin Lakes, NJ, USA) using the FL1 channel for green fluorescence (JC-1 monomers) and FL2 channel for red fluorescence (JC-1 aggregates). The red/green fluorescence ratio was determined as an indicator of changes in mitochondrial membrane potential. High red/green ratio (PE/FITC) ↑ → indicates high mitochondrial membrane potential and healthy mitochondrial function, whereas a low red/green ratio (PE/FITC) ↓ → indicates a disrupted mitochondrial membrane potential, indicative of mitochondrial damage or apoptosis.

Fluorescent Staining

The transfected I/R cells were seeded into culture dishes and incubated until reaching about 70% confluence. Cells were then incubated with the pre-prepared DCFH-DA staining solution (D6470, Solarbio, Beijing, China) at 37 °C for 30 minutes with gentle mixing. After staining, the cells were washed twice with PBS to remove excess dye. For nuclear counterstaining, cells were subsequently incubated with DAPI (4′,6-diamidino-2-phenylindole, 1 μg/mL) (C1006, Beyotime, Shanghai, China) for 5 minutes at room temperature in the dark. And fresh culture medium or PBS was added for fluorescence microscopy. Intracellular ROS production was examined using a fluorescence microscope (BX53, Olympus, Tokyo, Japan), and fluorescence intensity was quantitatively analyzed using ImageJ software (version 1.5f, NIH, Bethesda, MD, USA).

Statistical Analysis

Data were analyzed using GraphPad Prism software (version 9.0, GraphPad Software, Inc., San Diego, CA, USA). Data are presented as mean ± standard error of the mean (SEM). For comparisons among multiple groups, one-way ANOVA was applied, followed by Tukey's post-hoc test, unless otherwise specified. The number of mice included in the statistical analysis for each group was as follows: I/R, n = 6; Sham, n = 7; I/R+Gal-3, n = 5; I/R+anti-Gal-3, n = 7. However, comparisons between two groups

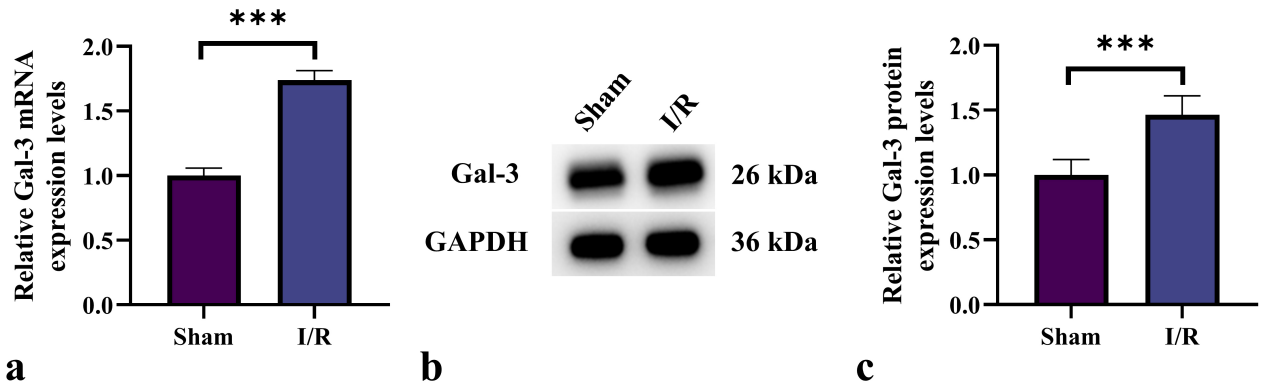

Fig. 1. Expression levels of Gal-3 in the I/R model. (a) mRNA expression levels of Gal-3 in the Sham and I/R groups. (b,c) Protein expression levels of Gal-3 in the Sham and I/R groups. Sample size: I/R = 6; Sham = 7. ***$p < 0.001$. I/R, ischemia-reperfusion.

were conducted using an unpaired two-tailed Student's *t*-test. A *p*-value of less than 0.05 was considered statistically significant.

Results

Evaluation of Gal-3 Expression in I/R

Initially, we evaluated the mRNA and protein expression levels of Gal-3 in the serum of I/R mice using qRT-PCR and Western blotting analysis. As depicted in Fig. 1a–c, compared to the Sham group, the I/R group demonstrated a significant upregulation of Gal-3 expression ($p < 0.05$).

Gal-3 Promotes Oxidative Stress and Inflammatory Response in I/R Mice

To elucidate the role of Gal-3 in the I/R model, human Gal-3 recombinant protein or Gal-3 antibody was injected into I/R mice. As shown in Fig. 2a,b, CK-MB and CK levels were substantially increased in the I/R group compared to the Sham group ($p < 0.05$). Moreover, Gal-3 treatment significantly elevated CK-MB and CK levels in the I/R+Gal-3 group ($p < 0.05$), whereas anti-Gal-3 treatment substantially reduced these levels in the I/R+anti-Gal-3 group ($p < 0.05$). These observations indicate that the Gal-3 recombinant protein exacerbates myocardial injury.

Cardiac function analysis showed that the I/R groups had considerably higher LVEDD and LVESD levels ($p < 0.05$) and lower LVEF and LVFS levels compared to the Sham group ($p < 0.05$) (Fig. 2c–f). Administration of Gal-3 further elevated LVEDD and LVESD levels ($p < 0.05$), while further reducing LVEF and LVFS levels ($p < 0.05$). In contrast, LVEDD and LVESD levels were significantly reduced, and LVEF and LVFS levels were increased in the I/R+anti-Gal-3 group ($p < 0.05$) compared to the I/R group.

HE staining showed that, compared to the Sham group, the I/R group exhibited significant tissue edema, extensive myocardial cell necrosis, increased infiltration of inflammatory cells, and greater vascular damage (Fig. 2g,h). These pathological changes were more pronounced in the I/R+Gal-3 group, whereas the I/R+anti-Gal-3 group displayed a significant reduction in these injuries.

Masson staining results indicated that, compared to the Sham group, myocardial fibrosis in the injury area was significantly increased in the I/R group (Fig. 3a,b). Fibrosis was further exacerbated after Gal-3 treatment, while anti-Gal-3 administration substantially decreased fibrotic deposition.

Evaluation of inflammatory cytokines revealed that the levels of IL-6, IFN-γ, and TNF-α were significantly elevated in the I/R group compared to the Sham group ($p < 0.05$) (Fig. 3c–e). Recombinant Gal-3 protein treatment further increased these cytokine levels ($p < 0.05$), whereas anti-Gal-3 treatment significantly reduced them ($p < 0.05$).

Analysis of oxidative stress markers showed that the I/R group exhibited significantly increased MDA levels and decreased SOD and GSH levels compared to the Sham group (Fig. 3f–h, $p < 0.05$). Recombinant Gal-3 protein treatment further increased MDA levels and decreased SOD and GSH levels ($p < 0.05$). In contrast, anti-Gal-3 treatment reversed these alterations, decreasing MDA levels and increasing SOD and GSH levels ($p < 0.05$).

Gal-3 Promotes an Inflammatory Response in the I/R Cell Model

We established an I/R model using human cardiomyocytes (AC16) and transfected the model cells with a Sh-Gal-3 or Gal-3 overexpression plasmid to modulate Gal-3 expression. As illustrated in Fig. 4a, Sh-Gal-3 significantly reduced Gal-3 mRNA expression levels in the I/R cell model, whereas Gal-3 overexpression plasmid significantly increased Gal-3 mRNA expression ($p < 0.05$). Additionally, in the I/R *in vitro* model, Gal-3 knockdown significantly reduced the levels of IL-1β, IL-6, TNF-α, and INF-γ, while Gal-3 overexpression significantly increased these inflammatory cytokines ($p < 0.05$) (Fig. 4b–e).

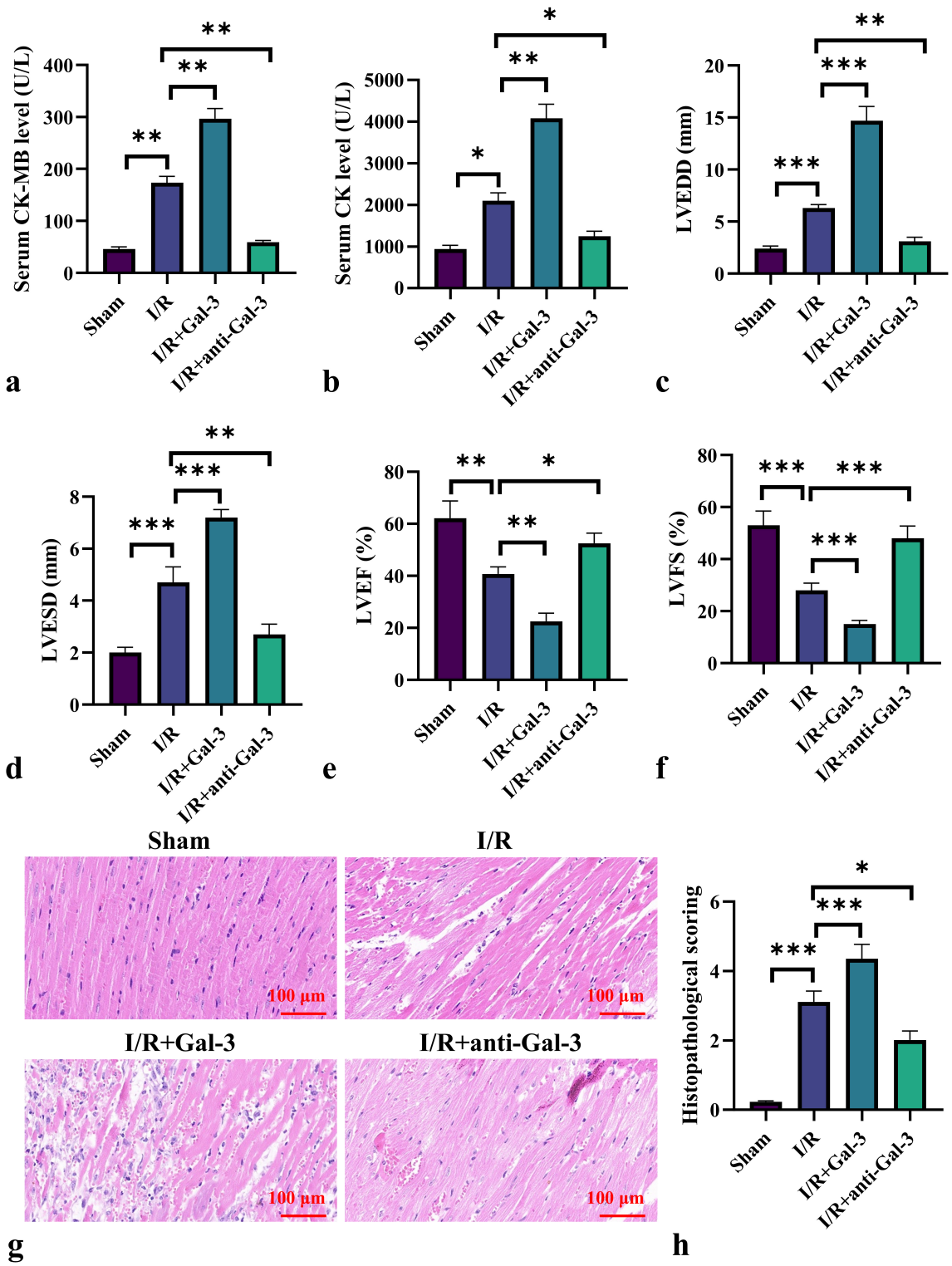

Fig. 2. Gal-3 exacerbates myocardial injury in I/R mice. (a,b) CK-MB and CK levels in mouse serum. (c–f) Levels of LVEDD, LVESD, LVEF, and LVFS in mice. (g,h) HE staining results of mouse cardiac tissue. Sample size: Sham = 7; I/R = 6; I/R+Gal-3 = 5; I/R+anti-Gal-3 = 7. *$p < 0.05$, **$p < 0.01$, ***$p < 0.001$. CK-MB, Creatine Kinase-MB; LVEDD, Left Ventricular End-Diastolic Diameter; LVESD, Left Ventricular End-Systolic Diameter; LVEF, Left Ventricular Ejection Fraction; LVFS, Left Ventricular Fractional Shortening; HE, Hematoxylin and Eosin.

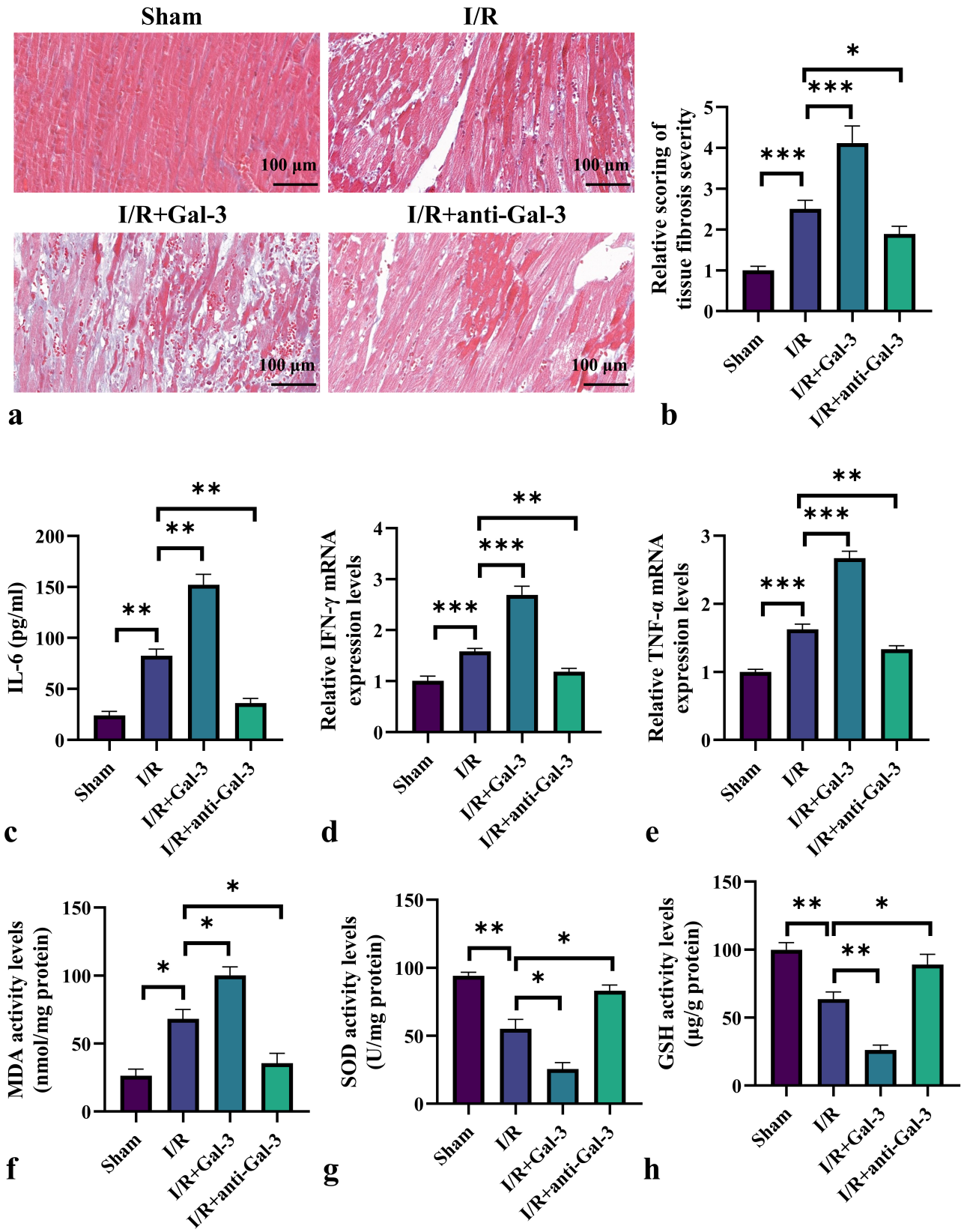

Fig. 3. Gal-3 regulates oxidative stress and inflammatory response in I/R mice. (a,b) Masson staining of mouse cardiac tissue. (c–e) Levels of IL-6, IFN-γ, and TNF-α in mouse cardiac tissue. (f–h) Levels of MDA, SOD, and GSH in mouse cardiac tissue. Sample size: Sham = 7; I/R = 6; I/R+Gal-3 = 5; I/R+anti-Gal-3 = 7. *$p < 0.05$, **$p < 0.01$, ***$p < 0.001$. IL-6, Interleukin-6; MDA, Malondialdehyde; SOD, Superoxide Dismutase; GSH, Glutathione.

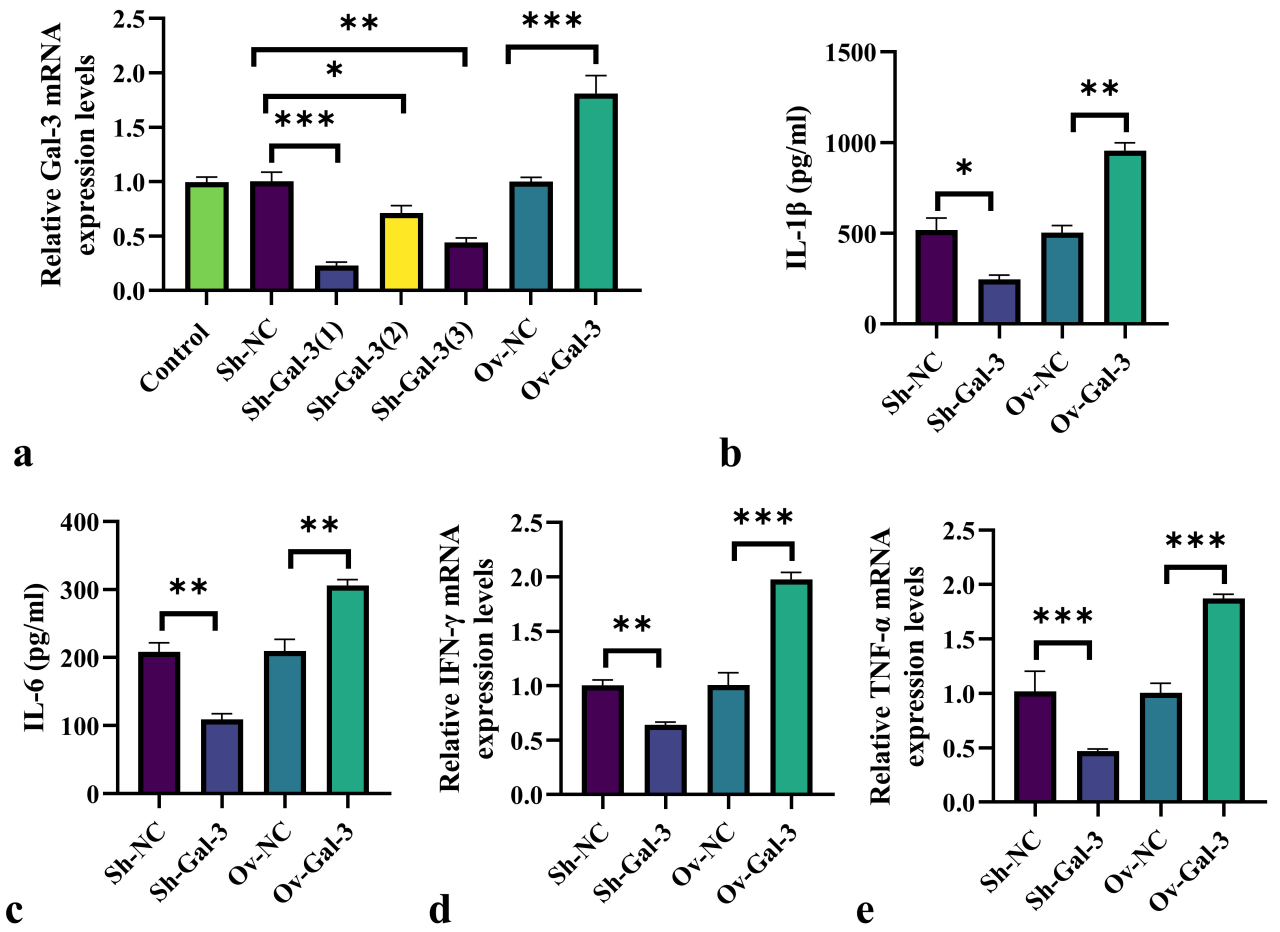

Fig. 4. Gal-3 promotes an inflammatory response in the I/R cell model. (a) Transfection efficiency verification after Gal-3 knockdown and overexpression in the I/R cell model. (b–e) Levels of IL-1β, IL-6, IFN-γ, and TNF-α in the I/R cell model. n = 6, *$p < 0.05$, **$p < 0.01$, ***$p < 0.001$.

Regulatory Effect of Gal-3 on Oxidative Stress in the I/R Cell Model

As shown in Fig. 5a–d, Gal-3 knockdown significantly reduced MDA levels and JC-1 disaggregation while substantially increasing SOD levels ($p < 0.05$). In contrast, Gal-3 overexpression significantly increased MDA levels and JC-1 disaggregation, whereas it decreased SOD levels ($p < 0.05$). Furthermore, Gal-3 knockdown significantly reduced ROS levels in the I/R cell model, whereas Gal-3 overexpression significantly increased ROS levels (Fig. 5e,f, $p < 0.05$).

Gal-3 Exerts a Disruptive Effect on the TFAM/PPARβ Signaling Axis

We assessed the protein expression levels of TFAM and PPARβ in the cardiac tissue of mice after different treatments. As depicted in Fig. 6a–c, compared to the Sham group, PPARβ levels were significantly increased and TFAM protein levels were significantly decreased in the I/R model group ($p < 0.05$). Compared to the I/R group, the I/R+Gal-3 group demonstrated further upregulation of PPARβ and downregulation of TFAM protein levels ($p < 0.05$), whereas in the I/R+anti-Gal-3 group, PPARβ protein expression was significantly reduced ($p < 0.05$), and TFAM expression was significantly increased ($p < 0.05$).

In the I/R *in vitro* cell model, Gal-3 knockdown significantly decreased PPARβ protein levels and increased TFAM levels. In contrast, Gal-3 overexpression significantly increased PPARβ and decreased TFAM protein levels (Fig. 6d–f, $p < 0.05$).

TFAM Mediates the Effect of Gal-3 in the I/R In Vitro Cell Model

To assess the correlation between TFAM and Gal-3, the I/R *in vitro* cell model was co-transfected with Sh-Gal-3 and Sh-TFAM (Fig. 7a–c). Compared to the Sh-NC group, Sh-Gal-3 treatment significantly increased the expression levels of TFAM protein and decreased the expression levels of PPARβ ($p < 0.05$). Conversely, the Sh-Gal-3+Sh-TFAM

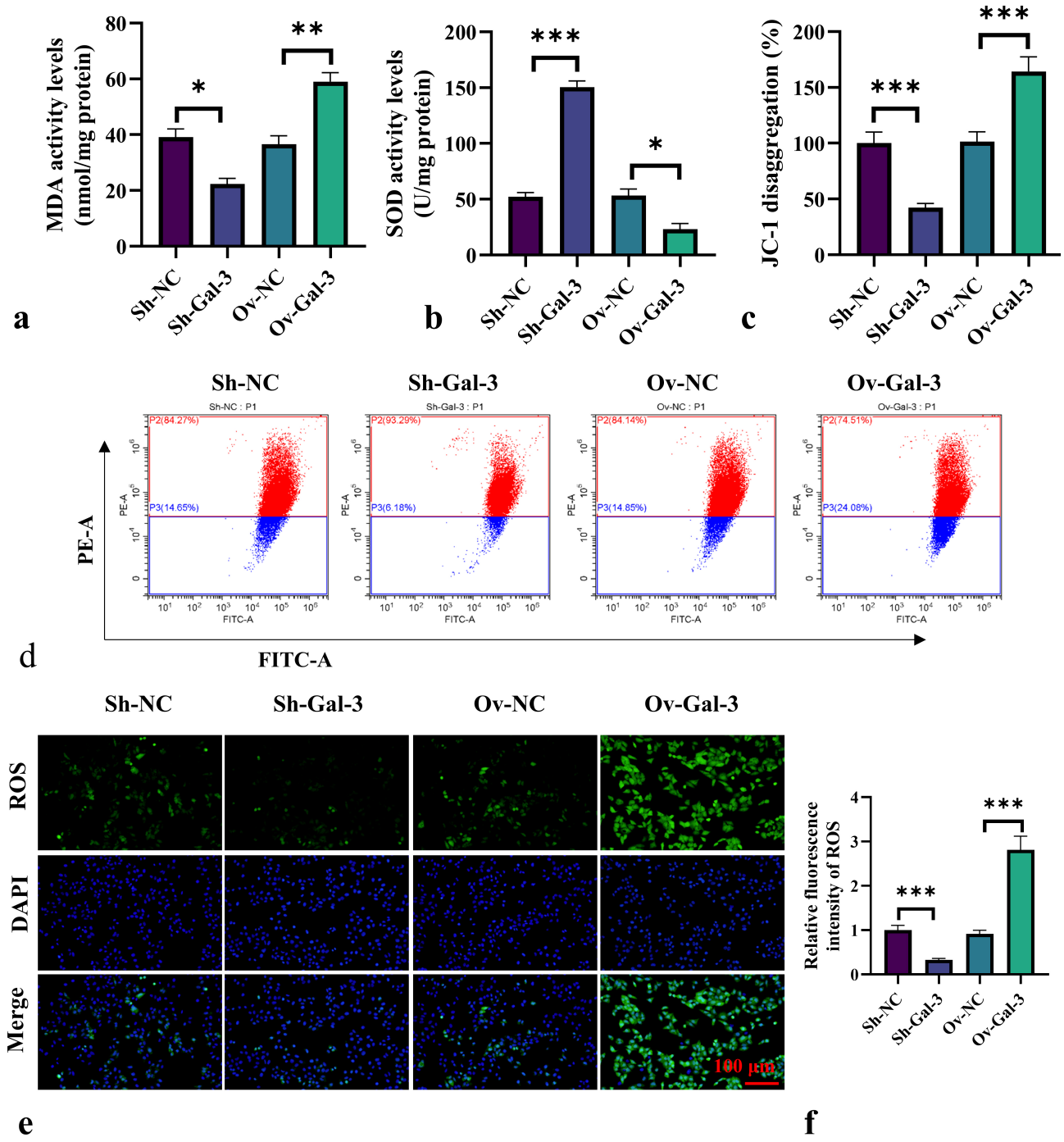

Fig. 5. Regulatory effect of Gal-3 on oxidative stress in the I/R cell model. (a–d) Effects of Gal-3 knockdown and overexpression on MDA, SOD, and JC-1 disaggregation levels in the I/R cell model. (e,f) Effects of Gal-3 knockdown and overexpression on ROS production levels in the I/R cell model. n = 6. *$p < 0.05$, **$p < 0.01$, ***$p < 0.001$. JC-1, 5,5′,6,6′-Tetrachloro-1,1′,3,3′-tetraethylbenzimidazolylcarbocyanine iodide; ROS, reactive oxygen species.

group substantially reduced TFAM protein expression and increased PPARβ levels compared to the Sh-Gal-3 group ($p < 0.05$).

Fig. 7d,e shows that Sh-Gal-3 treatment significantly reduced the fluorescence intensity of ROS in the I/R *in vitro* cell model ($p < 0.05$). In contrast, ROS fluorescence intensity was significantly higher in the Sh-Gal-3+Sh-TFAM group than in the Sh-Gal-3 group ($p < 0.05$).

Fig. 7f–h demonstrates that, compared to the Sh-Gal-3 group, Sh-Gal-3+Sh-TFAM treatment significantly in-

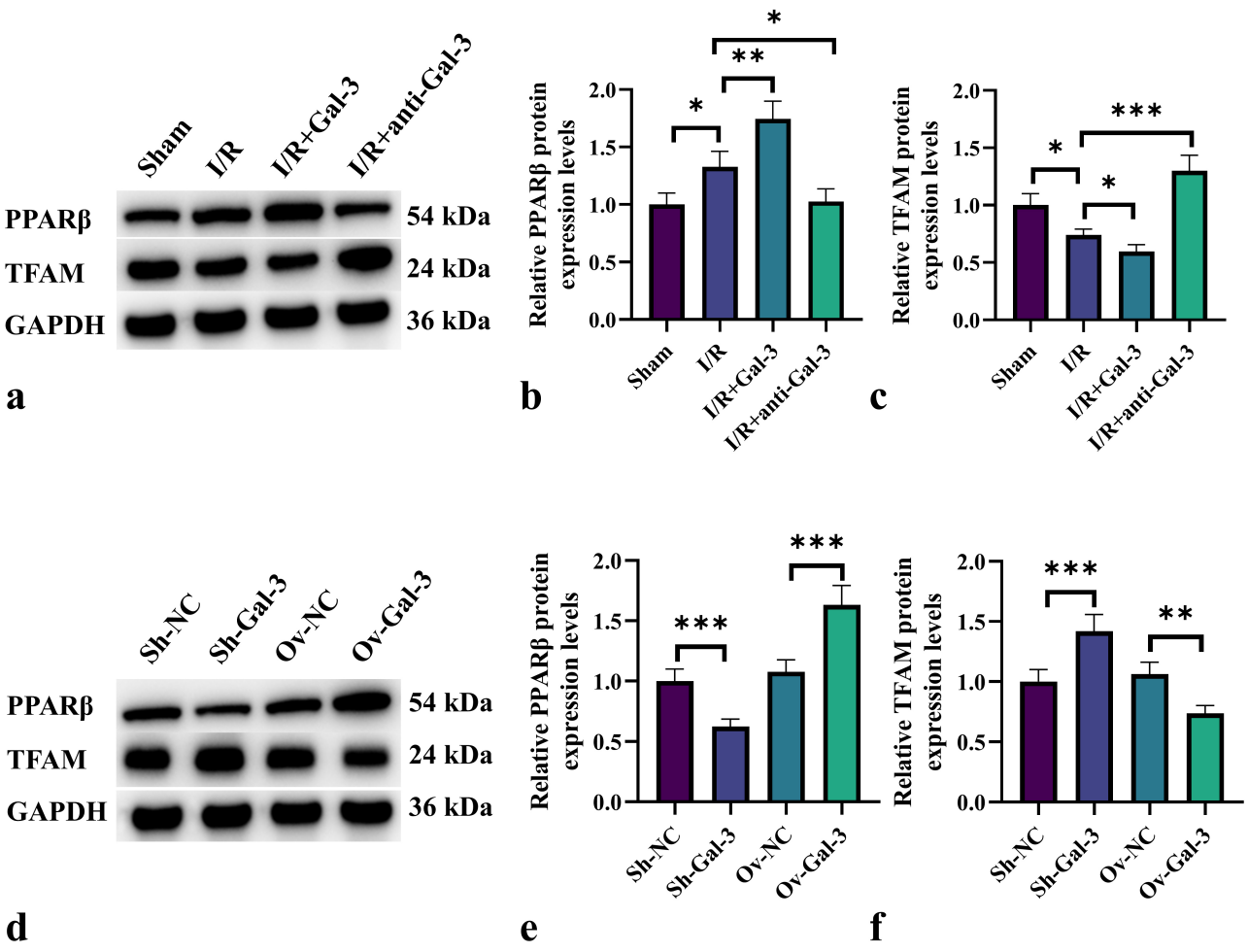

Fig. 6. Gal-3 exerts a disruptive effect on the TFAM/PPARβ signaling axis. (a–c) Expression levels of PPARβ and TFAM proteins in cardiac tissues of I/R mice treated with recombinant Gal-3 protein or Gal-3 antibody. (d–f) Expression levels of PPARβ and TFAM proteins in I/R *in vitro* cell models with Gal-3 knockdown or overexpression. Sample size: Sham = 7; I/R = 6; I/R+Gal-3 = 5; I/R+anti-Gal-3 = 7. Cell model: n = 6. *$p < 0.05$, **$p < 0.01$, ***$p < 0.001$. TFAM, mitochondrial transcription factor A; PPARβ, peroxisome proliferator-activated receptor β.

creased the levels of MDA and JC-1 disaggregation in the I/R *in vitro* cell model, while considerably decreasing SOD levels ($p < 0.05$). Furthermore, Sh-Gal-3+Sh-TFAM co-treatment significantly increased the levels of IL-6, IFN-γ, and TNF-α compared to the Sh-Gal-3 group (Fig. 7i–k).

Discussion

This study underscores the role of Gal-3 (galectin-3) in cardiac injury caused by ischemia-reperfusion (I/R), with a focus on its potential involvement in oxidative stress, inflammatory response, cell death, and cardiac remodeling. Our findings suggest that Gal-3 plays a key pathogenic role in I/R injury by enhancing oxidative stress, promoting inflammation, and exacerbating myocardial cell damage. Additionally, we observe that Gal-3 modulates myocardial injury by regulating the TFAM/PPARβ signaling pathway. These findings provide new insights into the role of Gal-3 in cardiovascular diseases and identify potential therapeutic targets aimed at reducing I/R-induced cardiac damage.

In this study, we observed a substantial upregulation of Gal-3 in the I/R mouse model, further underscoring its critical role in cardiovascular diseases. Gal-3 is known to be upregulated in various pathological conditions, particularly during inflammation, fibrosis, and cardiac lesions. Previous studies have shown that Gal-3 plays a critical role in cardiac injury by regulating immune responses and fibrosis through its interaction with glycosylated receptors [26,27]. Especially, in conditions such as acute myocardial injury and chronic heart failure, high Gal-3 expression levels are often associated with disease progression and poor prognosis [28]. Our study further demonstrates that Gal-3 expression increases during the early stages of I/R injury and is closely associated with the severity of myocardial damage.

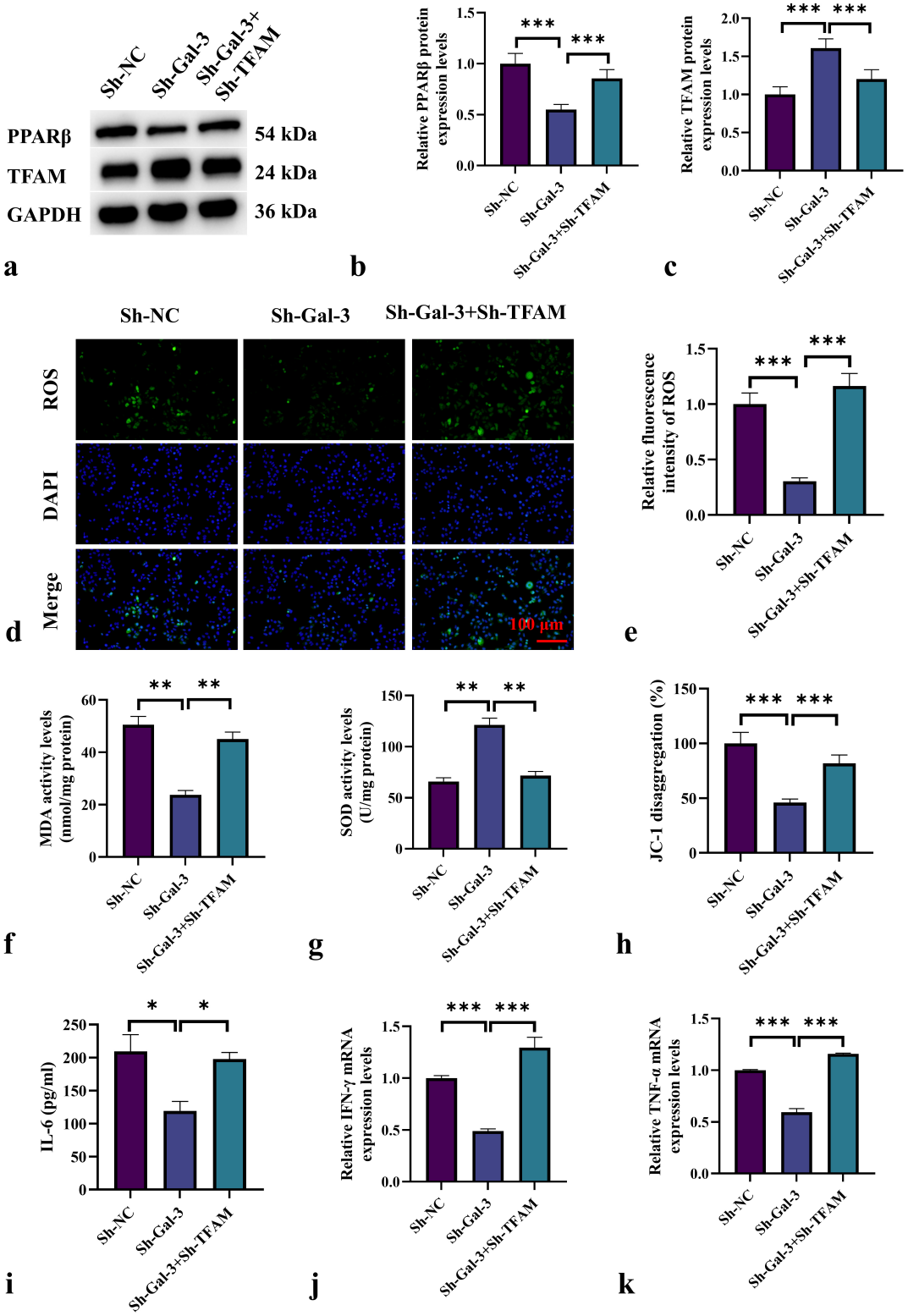

Fig. 7. TFAM mediates the effect of Gal-3 in the I/R *in vitro* cell model. (a–c) Effects of Sh-Gal-3 and Sh-TFAM on the expression of TFAM/PPARβ pathway proteins. (d,e) Effects of Sh-Gal-3 and Sh-TFAM on ROS production in I/R cells. (f–h) Effects of Sh-Gal-3 and Sh-TFAM on MDA, SOD, and JC-1 disaggregation levels in I/R cells. (i–k) Effects of Sh-Gal-3 and Sh-TFAM on IL-6, IFN-γ, and TNF-α levels in I/R cells. n = 6. *$p < 0.05$, **$p < 0.01$, ***$p < 0.001$.

These results suggest that Gal-3 may exacerbate cardiac injury by regulating multiple cellular processes, including inflammation, oxidative stress, and cell death.

In the I/R mouse model, we observed that Gal-3 significantly promoted oxidative stress and inflammatory responses, as evidenced by elevated MDA levels, reduced SOD and GSH levels, and higher ROS levels, thereby exacerbating myocardial cell damage. Previous studies have shown that oxidative stress plays a crucial role in I/R injury by promoting lipid peroxidation, disrupting cell membrane integrity, impairing mitochondrial function, and ultimately leading to cell death and tissue damage [29,30]. Gal-3 appears to exacerbate these effects, likely through activation of NADPH oxidase and enhanced ROS generation, thereby increasing the oxidative stress response [31]. Furthermore, anti-Gal-3 treatment significantly reduced MDA levels while increasing the activity of antioxidant enzymes such as SOD and GSH, suggesting that Gal-3 promotes oxidative stress by inhibiting endogenous antioxidant mechanisms.

In parallel, the pro-inflammatory role of Gal-3 was evident from the upregulation of pro-inflammatory cytokines, including IL-6, TNF-α, and IFN-γ. The inflammatory response is one of the key pathogenic mechanisms in I/R injury, contributing not only to the expansion of early myocardial damage but also being associated with subsequent cardiac remodeling, fibrosis, and functional loss [32]. In our study, Gal-3 increased cardiac inflammation by promoting immune cell activation and cytokine release, thereby exacerbating I/R-induced injury. Compared with existing evidence, this study reinforces the role of Gal-3 in the I/R model as a critical pro-inflammatory mediator, further validating its function as a key regulatory factor of cardiac inflammatory responses [33].

In this study, we further identified that Gal-3 influences I/R injury by modulating the TFAM/PPARβ signaling pathway. TFAM is crucial for maintaining mitochondrial genome stability and function, whereas PPARβ plays a vital role in regulating cellular metabolism, energy homeostasis, and redox balance [34]. Following I/R injury, Gal-3 modulated mitochondrial function and cellular energy metabolism by increasing PPARβ expression and decreasing TFAM expression. Hence, disruption in mitochondrial function and disturbances in cellular energy metabolism may lead to exacerbated myocardial cell damage. TFAM is a critical protective factor for mitochondrial DNA and is involved in mitochondrial replication and transcription. Therefore, its downregulation may impair mitochondrial function, further intensifying myocardial cell death [35].

The activation of PPARβ is typically associated with changes in fatty acid and energy metabolism and is recognized as cardioprotective [36]. However, excessive activation of PPARβ may disrupt cardiac metabolism, thereby further promoting I/R injury. Our study suggests that Gal-3 may disrupt the metabolic balance of cardiomyocytes by upregulating PPARβ, whereas anti-Gal-3 treatment significantly alleviates cardiac injury by restoring TFAM expression and reducing PPARβ levels. Previous study has reported that TFAM plays a protective role by maintaining mitochondrial DNA transcription and counteracting oxidative stress [11]. Meanwhile, PPARβ participates in energy metabolism and regulates inflammatory responses under cardiac stress [36]. Our results align with these findings and further reveal that Gal-3 disrupts the balance between these TFAM and PPARβ. Our findings uncover a new mechanism by which Gal-3 contributes to I/R injury, indicating its crucial role in cardiac injury and myocardial remodeling by influencing mitochondrial function and cellular energy metabolism.

By co-transfecting Sh-Gal-3 and Sh-TFAM into the I/R *in vitro* model, we further demonstrated the regulatory role of TFAM in Gal-3-mediated oxidative stress and inflammatory responses. Knockdown of Gal-3 led to upregulation of TFAM expression, which alleviated oxidative stress and inflammation, whereas knockdown of TFAM significantly enhanced the pro-oxidative stress effects of Gal-3. These observations indicate that TFAM plays a crucial regulatory role in mediating the effects of Gal-3 during I/R injury, likely by protecting mitochondrial function and maintaining cellular energy metabolism, thereby reducing oxidative damage. Therefore, TFAM not only plays a key role in cellular energy metabolism but may also regulate oxidative stress and cell death processes through its interaction with Gal-3.

This study reveals the crucial role of Gal-3 in I/R injury, particularly its potential involvement in promoting oxidative stress, driving inflammatory responses, and regulating mitochondrial function. Gal-3 represents a potential therapeutic target for cardiac diseases, especially acute myocardial injury and heart failure. Therapeutic approaches targeting Gal-3 may improve cardiac outcomes by alleviating inflammation, restoring antioxidant function, and maintaining mitochondrial integrity. Preclinical studies have already evaluated the application of Gal-3 inhibitors in cardiovascular diseases; for example, Olaratumab, a Gal-3 inhibitor, has demonstrated anti-inflammatory and antifibrotic potential in cancer models [37]. Therefore, future studies should explore the therapeutic efficacy of Gal-3 inhibitors in I/R injury and assess their potential synergy with other cardiovascular protective drugs.

Despite several valuable findings, we acknowledge some limitations in our study. First, the *in vitro* experiments were performed using a single cardiomyocyte cell line (AC16), which may not fully represent the complexity of the I/R cellular environment. Second, protein-level validation for TFAM and Gal-3 was limited due to technical challenges. Third, dosing of recombinant Gal-3 protein and antibody was based on preliminary experiments without published references, which may affect reproducibility. Finally, the long-term effects and potential compensatory

mechanisms following Gal-3 or TFAM modulation were not assessed and require further investigation.

Conclusions

This study systematically elucidates the mechanisms by which Gal-3 contributes to I/R-induced cardiac injury, demonstrating that Gal-3 exacerbates myocardial damage by promoting oxidative stress, stimulating inflammatory responses, and regulating the TFAM/PPARβ signaling pathway. Our findings provide new experimental evidence supporting the development of Gal-3-targeted therapeutic strategies and offer novel perspectives for treating myocardial I/R injury. Future research should further explore the interactions of Gal-3 with other key molecules and pathways to comprehensively understand its role in cardiac pathology and validate its potential as a therapeutic target.

Availability of Data and Materials

The data that support the findings of this study are available from the corresponding author upon reasonable request.

Author Contributions

TTL and JW designed the research study. TTL and JW performed the research. TTL collected and analyzed the data. TTL and JW have been involved in drafting the manuscript. Both authors have been involved in revising it critically for important intellectual content. Both authors gave final approval of the version to be published. Both authors have participated sufficiently in the work to take public responsibility for appropriate portions of the content and agreed to be accountable for all aspects of the work in ensuring that questions related to its accuracy or integrity.

Ethics Approval and Consent to Participate

This study has been approved by the Animal Ethics Committee of Binzhou Medical University (NO.2025-280).

Acknowledgment

Not applicable.

Funding

This research received no external funding.

Conflict of Interest

The authors declare no conflict of interest.

References

[1] Xiang Q, Yi X, Zhu XH, Wei X, Jiang DS. Regulated cell death in myocardial ischemia-reperfusion injury. Trends in Endocrinology and Metabolism. 2024; 35: 219–234. https://doi.org/10.1016/j.tem.2023.10.010.

[2] Zhang W, Zhang J, Wang Z, Li T, Liu C, Kang X, *et al*. Extracellular RIPK3 Acts as a Damage-Associated Molecular Pattern to Exaggerate Cardiac Ischemia/Reperfusion Injury. Circulation. 2024; 150: 1791–1811. https://doi.org/10.1161/CIRCULATIONAHA.123.068595.

[3] Wang J, Du H, Xie W, Bi J, Zhang H, Liu X, *et al*. CAR-Macrophage Therapy Alleviates Myocardial Ischemia-Reperfusion Injury. Circulation Research. 2024; 135: 1161–1174. https://doi.org/10.1161/CIRCRESAHA.124.325212.

[4] Hao T, Qian M, Zhang Y, Liu Q, Midgley AC, Liu Y, *et al*. An Injectable Dual-Function Hydrogel Protects Against Myocardial Ischemia/Reperfusion Injury by Modulating ROS/NO Disequilibrium. Advanced Science. 2022; 9: e2105408. https://doi.org/10.1002/advs.202105408.

[5] Zhu K, Fan R, Cao Y, Yang W, Zhang Z, Zhou Q, *et al*. Glycyrrhizin attenuates myocardial ischemia reperfusion injury by suppressing Inflammation, oxidative stress, and ferroptosis via the HMGB1-TLR4-GPX4 pathway. Experimental Cell Research. 2024; 435: 113912. https://doi.org/10.1016/j.yexcr.2024.113912.

[6] Yao Y, Li F, Zhang M, Jin L, Xie P, Liu D, *et al*. Targeting CaMKII-δ9 Ameliorates Cardiac Ischemia/Reperfusion Injury by Inhibiting Myocardial Inflammation. Circulation Research. 2022; 130: 887–903. https://doi.org/10.1161/CIRCRESAHA.121.319478.

[7] Zhang J, Liang R, Wang K, Zhang W, Zhang M, Jin L, *et al*. Novel CaMKII-δ Inhibitor Hesperadin Exerts Dual Functions to Ameliorate Cardiac Ischemia/Reperfusion Injury and Inhibit Tumor Growth. Circulation. 2022; 145: 1154–1168. https://doi.org/10.1161/CIRCULATIONAHA.121.055920.

[8] Algoet M, Janssens S, Himmelreich U, Gsell W, Pusovnik M, Van den Eynde J, *et al*. Myocardial ischemia-reperfusion injury and the influence of inflammation. Trends in Cardiovascular Medicine. 2023; 33: 357–366. https://doi.org/10.1016/j.tcm.2022.02.005.

[9] Liu Y, Li L, Wang Z, Zhang J, Zhou Z. Myocardial ischemia-reperfusion injury; Molecular mechanisms and prevention. Microvascular Research. 2023; 149: 104565. https://doi.org/10.1016/j.mvr.2023.104565.

[10] Chen LQ, Wang WS, Li SQ, Liu JH. Minocycline relieves myocardial ischemia-reperfusion injury in rats by inhibiting inflammation, oxidative stress and apoptosis. European Review for Medical and Pharmacological Sciences. 2022; 26: 3001–3009. https://doi.org/10.26355/eurrev_202204_28631.

[11] Rabinovich-Nikitin I, Rasouli M, Reitz CJ, Posen I, Margulets V, Dhingra R, *et al*. Mitochondrial autophagy and cell survival is regulated by the circadian *Clock* gene in cardiac myocytes during ischemic stress. Autophagy. 2021; 17: 3794–3812. https://doi.org/10.1080/15548627.2021.1938913.

[12] Zhao Q, Liu Z, Huang B, Yuan Y, Liu X, Zhang H, *et al*. PEDF improves cardiac function in rats subjected to myocardial ischemia/reperfusion injury by inhibiting ROS generation via PEDF R. International Journal of Molecular Medicine. 2018; 41: 3243–3252. https://doi.org/10.3892/ijmm.2018.3552.

[13] He H, Liu P, Li P. Dexmedetomidine Ameliorates Cardiac Ischemia/Reperfusion Injury by Enhancing Autophagy Through Activation of the AMPK/SIRT3 Pathway. Drug Design, Development and Therapy. 2023; 17: 3205–3218. https://doi.org/10.2147/DDDT.S428024.

[14] Huang P, Qu C, Rao Z, Wu D, Zhao J. Bidirectional regulation mechanism of TRPM2 channel: role in oxidative stress, inflammation and ischemia-reperfusion injury. Frontiers in Immunology. 2024; 15: 1391355. https://doi.org/10.3389/fimmu.2024.1391355.

[15] Procyk G, Czapla A, Jałocha K, Tymińska A, Grabowski M, Gąsecka A. The role of galectin-3 in atrial fibrillation. Journal of Molecular Medicine. 2023; 101: 1481–1492. https://doi.org/10.1007/s00109-023-02378-5.

[16] Chen Y, Fu W, Zheng Y, Yang J, Liu Y, Qi Z, *et al*. Galectin 3 enhances platelet aggregation and thrombosis via Dectin-1 activation: a translational study. European Heart Journal. 2022; 43: 3556–3574. https://doi.org/10.1093/eurheartj/ehac034.

[17] Horiuchi YU, Wettersten N, VAN Veldhuisen DJ, Mueller C, Filippatos G, Nowak R, *et al*. Galectin-3, Acute Kidney Injury and Myocardial Damage in Patients With Acute Heart Failure. Journal of Cardiac Failure. 2023; 29: 269–277. https://doi.org/10.1016/j.cardfail.2022.09.017.

[18] Soares LC, Al-Dalahmah O, Hillis J, Young CC, Asbed I, Sakaguchi M, *et al*. Novel Galectin-3 Roles in Neurogenesis, Inflammation and Neurological Diseases. Cells. 2021; 10: 3047. https://doi.org/10.3390/cells10113047.

[19] Zhang H, Feng Y, Si Y, Lu C, Wang J, Wang S, *et al*. Shank3 ameliorates neuronal injury after cerebral ischemia/reperfusion via inhibiting oxidative stress and inflammation. Redox Biology. 2024; 69: 102983. https://doi.org/10.1016/j.redox.2023.102983.

[20] Jiang L, Yin X, Chen YH, Chen Y, Jiang W, Zheng H, *et al*. Proteomic analysis reveals ginsenoside Rb1 attenuates myocardial ischemia/reperfusion injury through inhibiting ROS production from mitochondrial complex I. Theranostics. 2021; 11: 1703–1720. https://doi.org/10.7150/thno.43895.

[21] Barman SA, Bordan Z, Batori R, Haigh S, Fulton DJR. Galectin-3 Promotes ROS, Inflammation, and Vascular Fibrosis in Pulmonary Arterial Hypertension. Advances in Experimental Medicine and Biology. 2021; 1303: 13–32. https://doi.org/10.1007/978-3-030-63046-1_2.

[22] Li ZZ, Guo L, An YL, Yu WJ, Shi DY, Lin QY, *et al*. Evolocumab attenuates myocardial ischemia/reperfusion injury by blocking PCSK9/LIAS-mediated cuproptosis of cardiomyocytes. Basic Research in Cardiology. 2025; 120: 301–320. https://doi.org/10.1007/s00395-025-01100-5.

[23] Mikolka P, Kosutova P, Balentova S, Cierny D, Kopincova J, Kolomaznik M, *et al*. Early cardiac injury in acute respiratory distress syndrome: comparison of two experimental models. Physiological Research. 2020; 69: S421–S432. https://doi.org/10.33549/physiolres.934591.

[24] Guo J, Wang S, Wan X, Liu X, Wang Z, Liang C, *et al*. Mitochondria-derived methylmalonic acid aggravates ischemia-reperfusion injury by activating reactive oxygen species-dependent ferroptosis. Cell Communication and Signaling. 2024; 22: 53. https://doi.org/10.1186/s12964-024-01479-z.

[25] Xin Y, Su P, Liu Y, Gu S, An X, Zhang X, *et al*. Knock out hepatic Krüppel-like factor 16 (KLF16) improve myocardial damage and promoted myocardial protection of myocardial ischemia-reperfusion via anti-oxidative and anti-inflammation effects by TFAM/PPARβ signal passage. Bioengineered. 2021; 12: 10219–10231. https://doi.org/10.1080/21655979.2021.1982302.

[26] Seropian IM, Fontana Estevez FS, Villaverde A, Cacciagiú L, Bustos R, Touceda V, *et al*. Galectin-3 contributes to acute cardiac dysfunction and toxicity by increasing oxidative stress and fibrosis in doxorubicin-treated mice. International Journal of Cardiology. 2023; 393: 131386. https://doi.org/10.1016/j.ijcard.2023.131386.

[27] Al-Salam S, Kandhan K, Sudhadevi M, Yasin J, Tariq S. Early Doxorubicin Myocardial Injury: Inflammatory, Oxidative Stress, and Apoptotic Role of Galectin-3. International Journal of Molecular Sciences. 2022; 23: 12479. https://doi.org/10.3390/ijms232012479.

[28] Zhang Y, Xiong X, Wang J, Guo F. Prognostic value of serum IGF-1, Gal-3, and PTX-3 levels in elderly patients with chronic heart failure. American Journal of Translational Research. 2024; 16: 1393–1400. https://doi.org/10.62347/ZOMD7815.

[29] Kong CY, Guo Z, Song P, Zhang X, Yuan YP, Teng T, *et al*. Underlying the Mechanisms of Doxorubicin-Induced Acute Cardiotoxicity: Oxidative Stress and Cell Death. International Journal of Biological Sciences. 2022; 18: 760–770. https://doi.org/10.7150/ijbs.65258.

[30] Chen Y, Guo X, Zeng Y, Mo X, Hong S, He H, *et al*. Oxidative stress induces mitochondrial iron overload and ferroptotic cell death. Scientific Reports. 2023; 13: 15515. https://doi.org/10.1038/s41598-023-42760-4.

[31] Li M, Tian M, Jiang X, Liu Y, Wang Y, Li Y. Inhibition of galectin-3 ameliorates high-glucose-induced oxidative stress and inflammation in ARPE-19 cells. Cutaneous and Ocular Toxicology. 2022; 41: 179–186. https://doi.org/10.1080/15569527.2022.2081701.

[32] Feng ZJ, Wang LS, Ma X, Li K, Li XY, Tang Y, *et al*. Catapol attenuates the aseptic inflammatory response to hepatic I/R injury in vivo and in vitro by inhibiting the HMGB1/TLR-4/NF-κB signaling pathway via the microRNA-410-3p. Molecular Immunology. 2023; 164: 66–78. https://doi.org/10.1016/j.molimm.2023.11.004.

[33] Luo Y, Cheng J, Fu Y, Zhang M, Gou M, Li J, *et al*. D-allose Inhibits TLR4/PI3K/AKT Signaling to Attenuate Neuroinflammation and Neuronal Apoptosis by Inhibiting Gal-3 Following Ischemic Stroke. Biological Procedures Online. 2023; 25: 30. https://doi.org/10.1186/s12575-023-00224-z.

[34] Ivraghi MS, Zamanian MY, Gupta R, Achmad H, Alsaab HO, Hjazi A, *et al*. Neuroprotective effects of gemfibrozil in neurological disorders: Focus on inflammation and molecular mechanisms. CNS Neuroscience & Therapeutics. 2024; 30: e14473. https://doi.org/10.1111/cns.14473.

[35] Boovarahan SR, Balu K, Prem P, Sivakumar B, Kurian GA. DNA hypomethylation by fisetin preserves mitochondria functional genes and contributes to the protection of I/R rat heart. Functional & Integrative Genomics. 2023; 23: 325. https://doi.org/10.1007/s10142-023-01257-z.

[36] Papatheodorou I, Galatou E, Panagiotidis GD, Ravingerová T, Lazou A. Cardioprotective Effects of PPARβ/δ Activation against Ischemia/Reperfusion Injury in Rat Heart Are Associated with ALDH2 Upregulation, Amelioration of Oxidative Stress and Preservation of Mitochondrial Energy Production. International Journal of Molecular Sciences. 2021; 22: 6399. https://doi.org/10.3390/ijms22126399.

[37] Mascarenhas L, Ogawa C, Laetsch TW, Weigel BJ, Bishop MW, Krystal J, *et al*. Phase 1 trial of olaratumab monotherapy and in combination with chemotherapy in pediatric patients with relapsed/refractory solid and central nervous system tumors. Cancer Medicine. 2021; 10: 843–856. https://doi.org/10.1002/cam4.3658.